Journal of Sound and Vibration (1999) **226**(1), 25–39
Article No. jsvi.1999.2162, available online at http://www.idealibrary.com on IDEAL®

HYBRID $\mathcal{H}_2$ CONTROL DESIGN FOR VIBRATION ISOLATION

T. E. PARÉ

Department of Mechanical Engineering, Stanford University, Stanford, CA 94035, *U.S.A.*

AND

J. P. HOW

Department of Aeronautics and Astronautics, Stanford University, Stanford, CA 94035, *U.S.A.*

(*Received* 21 *May* 1998, *and in final form* 8 *February* 1999)

Combined feedforward and feedback (hybrid) controller design has recently been shown to be an effective approach for acoustic and structural vibration control. This paper extends previous analysis of this architecture to investigate the strong coupling that typically exists between the feedforward and feedback components for a system having noise on the feedforward sensor. One shows with a simple structural isolation example that the optimal hybrid $\mathcal{H}_2$ controller offers the benefit of simultaneous improvement in vibration performance along with a reduction in closed loop control bandwidth.

1. INTRODUCTION

Of recent interest in the field of vibration control and suppression is the design of control systems that use both feedforward and feedback sensors [1–3]. Within this architecture, the feedback sensor provides some measure of the system response, and the feedforward sensor provides a measure of the disturbance. A controller designed to utilize a combination of feedforward and feedback sensors has been called a *hybrid* controller [4].

In this paper one looks specifically at hybrid control designs that optimize an $\mathcal{H}_2$ performance objective. The problem of interest is to determine the degree of coupling that exists between the feedforward and feedback controllers within this architecture. Reference [4] considered a similar problem for the special case with no noise on the feedforward sensor. The results in reference [4] show that the feedforward and feedback design problems are separable, i.e., the feedback controller can be designed independently of the feedforward controller. These results are extended here to the more general case of sensor noise on the feedforward sensor, for which the feedforward and feedback control design

0022–460X/99/360025 + 15 $30.00/0

problems are explicitly shown to be coupled. In addition, it is demonstrated that the feedforward sensor offers design freedom that can be exploited to improve the $\mathcal{H}_2$ performance while simultaneously reducing the loop bandwidth. This reduction in the loop bandwidth can provide an increase in stability robustness for uncertain high frequency dynamics, which is a key issue for active structural (acoustic) controllers [3, 5–7]. This paper provides a thorough investigation of this coupling in the realistic case of non-zero noise on a feedforward sensor, which is a key step for general hybrid $\mathcal{H}_2$ controllers. Note that one of the advantages of designing the combined controllers within an optimization framework such as $\mathcal{H}_2$ or $\mathcal{H}_\infty$, is that parametric robustness can also be included in the control designs [8–10]. Also, using the $\mathcal{H}_2$ frequency weighted cost functionals in references [11–13], the feedforward component of the controllers can be designed to cancel harmonic disturbances. Thus, a full understanding of the synergistic coupling that exists in the realistic case of non-zero noise on a feedforward sensor is extremely important for hybrid design, and it is toward this end that this paper provides a thorough investigation.

The paper is organized as follows. Section 2 presents the $\mathcal{H}_2$ controller specific to the two sensor configuration, using a development that parallels that described in reference [4]. This more general development is included in detail for completeness and also for the purpose of deriving the analytic form of the two-input hybrid controller for a simple scalar system. This particular controller is then used in section 3 to illustrate the design freedom offered by the two sensor approach. This analysis is done in the form of various trade-offs between system parameters such as $\mathcal{H}_2$ performance and control bandwidth versus the noise parameters of the sensors. Section 4 presents a more realistic example to evaluate the trends in a system with sensor dynamics.

2. $\mathcal{H}_2$ OPTIMAL SOLUTION: THE TWO RICCATI EQUATIONS

In this section it is shown how a system with a combination of feedforward and feedback sensors can be cast into the LQG framework. The standard set-up for this problem is shown in Figure 1. The measurement $y(t)$ is comprised of two parts, y_{m1} and y_{m2}, given by the feedback and feedforward sensors, respectively. These sensors have white noise, $\eta_1(t)$ and $\eta_2(t)$ with spectral density matrices V_{ms} and V_p, respectively. Using the notation of reference [4], the system is acted upon with two disturbances, a random white noise $w_r(t)$, and a measurable white noise $w_m(t)$. For simplicity in the presentation, one assumes that all white noises are zero mean and mutually uncorrelated. Assuming a state space representation for the linear system, $G{:}u \to y_p$ is given by

$$G(s) \stackrel{s}{:=} \left[\begin{array}{cc} A & B_u \\ C_{y_p} & D_{yu} \end{array}\right], \tag{1}$$

the system dynamics shown in Figure 1 can be written as

$$\dot{x} = Ax + B_u u + [B_r \quad B_m \quad 0 \quad 0] \begin{bmatrix} w_r \\ w_m \\ \eta_1 \\ \eta_2 \end{bmatrix} = Ax + B_u u + B_w w. \tag{2}$$

The measurement $y(t) = [y_{m1}^{\mathrm{T}} \quad y_{m2}^{\mathrm{T}}]^{\mathrm{T}}$ can then be expressed as

$$y = \begin{bmatrix} C_{y_p} \\ 0 \end{bmatrix} x + \begin{bmatrix} 0 & 0 & D_p & 0 \\ 0 & I & 0 & D_{ms} \end{bmatrix} \begin{bmatrix} w_r \\ w_m \\ \eta_1 \\ \eta_2 \end{bmatrix} = C_y x + D_{yw} w, \tag{3}$$

where unity weighting has been assumed on the disturbance vector $\mathbf{w}_m$. The performance variable of interest is defined to be the output $z(t)$, with

$$z = C_z x + D_{zu} u. \tag{4}$$

The objective is to control $z(t)$ using the control signal $u(t)$ in the presence of all disturbances $w(t)$. With these definitions one then has completely defined a state space realization for the standard two-port system [14, p. 87] $\bar{G}(s)$,

$$\bar{G} = \begin{bmatrix} G_{zw} & G_{zu} \\ G_{yw} & G_{yu} \end{bmatrix}, \tag{5}$$

shown in Figure 2.

The optimal $\mathcal{H}_2$ solution to this problem requires the minimization of the functional (see for example reference [15, pp. 278–280]),

$$J_{LQG} = \lim_{t \to \infty} E[z^{\mathrm{T}}(t) z(t)] \triangleq \|z\|_{RMS}^2. \tag{6}$$

As is well known, when only the output $y(t)$ is available, the optimal controller is linear and requires the solution of a pair of Riccati equations corresponding to the linear quadratic estimation (LQE) and regulation (LQR) problems. In terms of the given state space representation for $\bar{G}(s)$, the LQR and LQE Riccati equations are

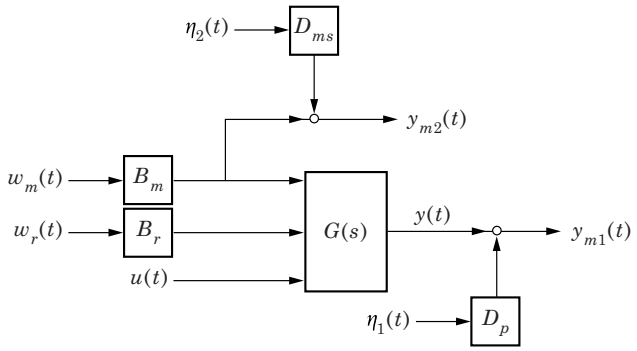

Figure 1. Hybrid control set-up.

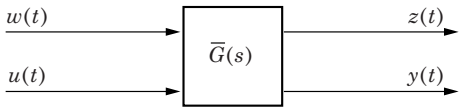

Figure 2. Standard two-part $\mathcal{H}_2$ control system, $\bar{G}$.

$$0 = (A - B_u R_2^{-1} R_{12}^{\mathrm{T}})^{\mathrm{T}} P + P(A - B_u R_2^{-1} R_{12}^{\mathrm{T}}) - P B_u R_2^{-1} B_u^{\mathrm{T}} P + R_1 - R_{12} R_2^{-1} R_{12}^{\mathrm{T}} \tag{7}$$

and

$$0 = (A - V_{12} V_2^{-1} C_y) Q + Q(A - V_{12} V_2^{-1} C_y)^{\mathrm{T}} - Q C_y^{\mathrm{T}} V_2^{-1} C_y Q + V_1 - V_{12} V_2^{-1} V_{12}^{\mathrm{T}}, \tag{8}$$

where

$$R_1 = C_z^{\mathrm{T}} C_z, \quad R_{12} = C_z^{\mathrm{T}} D_{zw} = 0, \quad R_2 = D_{zu}^{\mathrm{T}} D_{zu},$$

$$V_1 = B_w B_w^{\mathrm{T}}, \quad V_{12} = B_w D_{yw}^{\mathrm{T}}, \quad V_2 = D_{yw} D_{yw}^{\mathrm{T}}.$$

The state space solution of the controller (11) is straightforward given the solution P and Q of the Riccati equations (7, 8). The controller matrices are

$$A_c = A + B_u C_c - B_c C_y, \quad B_c = (Q C_y^{\mathrm{T}} + V_{12}) V_2^{-1}, \quad C_c = -R_2^{-1}(B_u^{\mathrm{T}} P + R_{12}^{\mathrm{T}}). \tag{9–11}$$

Note that these expressions assume no coupling between the state and control components of the performance ($R_{12} = 0$), and that the resulting controller is strictly proper, i.e., $D_c = 0$.

2.1. THE HYBRID $\mathcal{H}_2$ CONTROLLER

The following provides an analysis of the behavior of the hybrid controller developed in the previous section. One first identifies the impact of the sensor parameters on the solution of the LQE Riccati equation (8). By definition,

$$V_1 = B_r B_r^{\mathrm{T}} + B_m B_m^{\mathrm{T}} = V_r + V_m, \quad V_{12} = [0 \quad B], \tag{12}$$

$$V_2 = \begin{bmatrix} D_p D_p^{\mathrm{T}} & 0 \\ 0 & I + D_{ms} D_{ms}^{\mathrm{T}} \end{bmatrix} = \begin{bmatrix} V_p & 0 \\ 0 & I + V_{ms} \end{bmatrix}. \tag{13}$$

Then, similarly to reference [4], one has that

$$V_{12} V_2^{-1} C = [0 \quad B_m] \begin{bmatrix} V_p^{-1} & 0 \\ 0 & (I + V_{ms})^{-1} \end{bmatrix} \begin{bmatrix} C_y \\ 0 \end{bmatrix} = 0,$$

and

$$V_{12}V_2^{-1}V_{12}^{\mathrm{T}} = B_m(I + V_{ms})^{-1}B_m^{\mathrm{T}}. \tag{14}$$

With the above substitutions into equation (8),

$$\begin{aligned} 0 &= AQ + QA - QC_y^{\mathrm{T}}V_p^{-1}C_yQ + V_r + V_m - B_m(I + V_{ms})^{-1}B_m^{\mathrm{T}} \\ &= AQ + QA - QC_y^{\mathrm{T}}V_p^{-1}C_yQ + V_e, \end{aligned} \tag{15}$$

where the *effective* process noise for the system V_e is

$$V_e = V_r + V_m - B_m(I + V_{ms})^{-1}B_m^{\mathrm{T}} = V_r + B_m(V_{ms}(I + V_{ms})^{-1})B_m^{\mathrm{T}}. \tag{16}$$

In this expression, $V_1 = V_r + V_m$ corresponds to the amount of process noise acting on the system. However, equation (16) shows that this amount is effectively reduced when the feedforward sensor is used. Of course, the effective reduction is a function of the relative "quality" of the feedforward measurement, given by V_{ms}. Reference [4] considers the case with $V_{ms} = 0$ (a perfect feedforward sensor) which yields the maximal reduction in V_e and separability of the controllers. Stronger coupling exists between the two designs for systems that have feedforward sensor noise, and the following sections provide further insights on the degree of coupling that exists.

2.2. SPECIAL CASE: SCALAR SYSTEM

In order to further understand the effect of the feedforward on the resulting controller, a simple scalar system with scalar inputs and outputs is considered. The system dynamics are described by

$$\dot{x} = ax + b_u u + b_w w = ax + u + [0 \quad b_m \quad 0 \quad 0]\begin{bmatrix} w_r \\ w_m \\ \eta_1 \\ \eta_2 \end{bmatrix}. \tag{17}$$

The measurement is

$$y = C_y x + D_{yw} w = \begin{bmatrix} 1 \\ 0 \end{bmatrix} x + \begin{bmatrix} 0 & 0 & d_p & 0 \\ 0 & 1 & 0 & d_{ms} \end{bmatrix}\begin{bmatrix} w_r \\ w_m \\ \eta_1 \\ \eta_2 \end{bmatrix}, \tag{18}$$

and the scalar performance is given by

$$z = c_z x + b_{zu} u. \tag{19}$$

It is easily shown then that the LQR Riccati equation (7) for this system reduces to

$$0 = 2ap - p^2/r_2 + r_1, \tag{20}$$

for which the optimal solution is

$$p_o = ar_2 + \sqrt{a^2 r_2^2 + r_1 r_2}, \tag{21}$$

where $r_1 = c_z^2$ and $r_2 = b_{zu}^2$. Similarly, the optimal LQE equation (8) reduces to

$$0 = 2aq - q^2/v_p + v_e, \tag{22}$$

where

$$v_e = v_r + v_m v_{ms}/(1 + v_{ms}). \tag{23}$$

and the optimal LQE solution is given as

$$q_o = av_p + \sqrt{a^2 v_p^2 + v_p v_e}. \tag{24}$$

With these exact Riccati solutions the explicit formula for two-input controller is obtained by simplifying equation (11):

$$\begin{aligned} K(s) &= \frac{-(a + \sqrt{a^2 + r_1/r_2})}{s + a + \sqrt{a^2 + r_1/r_2} + \sqrt{a^2 + v_e/v_p}} \left[a + \sqrt{a^2 + v_e/v_p} \middle| \frac{b_m}{1 + v_{ms}} \right] \\ &= [K_{fb}(s) \quad | \quad K_{ff}(s)]. \end{aligned} \tag{25}$$

For this simple problem, equation (25) explicitly shows the role of the feedforward sensor noise in the optimal blending of the feedforward and feedback controllers, and in the modifications to the feedback controller bandwidth and low frequency gain. Several special cases are of interest.

1. Note that a noisier measurement of the disturbance corresponds to an increase in the v_{ms}. Equation (25) indicates that in this case, the feedforward component K_{ff} is effectively *shut off* because the coefficient $b_m/(1 + v_{ms})$ is inversely proportional to v_{ms}. Furthermore, the effective process noise $V_e \approx V_1$, and, as expected, the controller reduces to the standard $\mathcal{H}_2$ feedback design.
2. Another interesting case occurs for an ideal feedforward sensor, i.e., $v_{ms} \to 0$. In this case $v_e \to v_r$, and thus the noise intensity associated with the measured disturbance is reduced. The measured disturbance can then be treated as a deterministic signal and incorporated into the feedback controller with full gain b_m. As $v_{ms} \to 0$, K_{fb} becomes the standard $\mathcal{H}_2$ controller, designed with process noise intensity $v_r < v_1$ [4].

These two extreme cases illustrate a key trend in the combined design, namely that the optimal feedforward and feedback controllers both depend on the feedforward sensor sensor noise. For example, reducing v_{ms} also reduces the effective process noise v_e. This change results in a lower feedback loop gain, a slower controller pole, and an increased use of the feedforward sensor. The next section discusses the impact of these changes to the two controllers on the disturbance rejection performance of the closed-loop system.

3. NUMERICAL ANALYSIS

The scalar system in the previous section can be used to investigate the control architecture design trade-offs in the design of hybrid $\mathcal{H}_2$ controllers. Specifically the effects of the feedback and feedforward sensor noise on the closed loop bandwidth and $\mathcal{H}_2$ performance are considered. The optimal $\mathcal{H}_2$ cost for a system can be written as

$$J_{LQG} = \mathrm{Tr}\{PV_e + QK_{LQR}^{\mathrm{T}} R_2 K_{LQR}\}, \tag{26}$$

where the LQR feedback gain matrix $K_{LQR} = -R_2^{-1} B_u^{\mathrm{T}}$. For the scalar system this reduces to

$$J_{LQC} = p_o v_e + q_o p_o^2 / r_2. \tag{27}$$

For simplicity, the highest loop crossover frequency,

$$w_c = \{\omega \mid |G_{yu}(\mathrm{j}\omega) K_{fb}(\mathrm{j}\omega)| = 1\},$$

is used as the criterion for evaluating system bandwidth. In terms of the system parameters the crossover frequency is

$$2\omega_c^2 = -(a^2 + \beta^2) + \sqrt{(a^2 + \beta^2) + 4\{(a^2 + l_1^2)^2 (a^2 + l_2^2)^2 - a^2 \beta^2\}}, \tag{28}$$

where $l_1 = \sqrt{a^2 + r_1/r_2}$, $l_2 = \sqrt{a^2 + v_e/v_p}$ and $\beta = a + l_1 + l_2$. Note that only the feedback controller influences the crossover frequency, but the compensator gain is changed when one introduces the feedforward sensor. The impact of the feedforward sensor is seen explicitly in equation (28) since V_{ms} will change V_e.

3.1. COST AND BANDWIDTH VERSUS SENSOR NOISE INTENSITY

For this trade study the parameters of the scalar system will be fixed simply as $a = 1$, $b_w = b_{zu} = c_z = 1$ and the LQG weights as $r_1 = 1$, $r_2 = 1$, $v_m = 10$, $v_r = 1$, and the effects of varying feedforward and feedback sensor noise on the performance cost and loop bandwidth are examined, as defined above. These effects are shown in Figures 3 and 4.

In Figure 3, the performance and control bandwidths are graphed as a function of feedback sensor noise intensity for various levels of feedforward sensor noise. As expected, the performance degrades as the feedback sensor noise increases. The nearly linear behavior with v_p is consistent with the linear dependence of the cost (27) on the Riccati solution (24). The crossover frequency decreases with increasing feedback sensor noise, which corresponds to a decrease in controller authority and in essence, less reliance by the controller on the feedback information. These trends are common in any control design process. However, Figure 3 can also be used to analyze the impact of the feedforward sensor as well. In particular, Figure 3 shows that, while the bandwidth decreases for increasing feedback sensor noise v_p, the bandwidth curves *increase* for increasing levels of feedforward sensor noise v_{ms}. Thus as v_{ms} increases, there is less reliance on the feedforward component in the optimal design resulting in a higher bandwidth feedback design. Conversely, as the noise on the feedforward

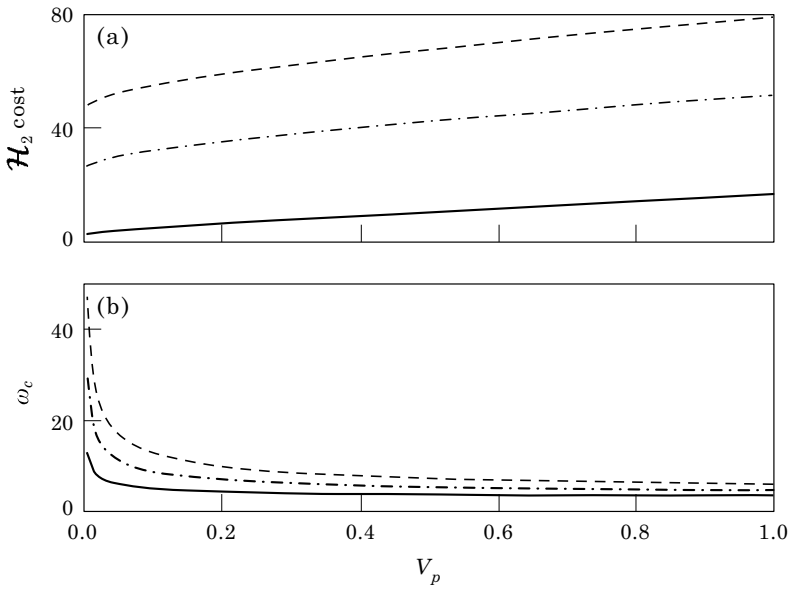

Figure 3. Performance and bandwidth trends as a function of feedback sensor noise intensity. (a) $\mathcal{H}_2$ performance; (b) W_c as a function of V_p. (—, $V_{ms} = 0{\cdot}1$; –·–, $V_{ms} = 1{\cdot}0$; - - -, $V_{ms} = 10$.)

sensor is reduced one sees a marked reduction in the feedback controller bandwidth.

Figure 4 also shows the impact of the relative noise levels of the feedback and feedforward sensors on the resulting bandwidth (as measured by the loop crossover) and the system $\mathcal{H}_2$ performance. For a fixed feedforward sensor noise intensity V_{1m}, the performance of the system should improve with higher quality feedback signal y_m. This improvement is seen in the figure with the $\mathcal{H}_2$

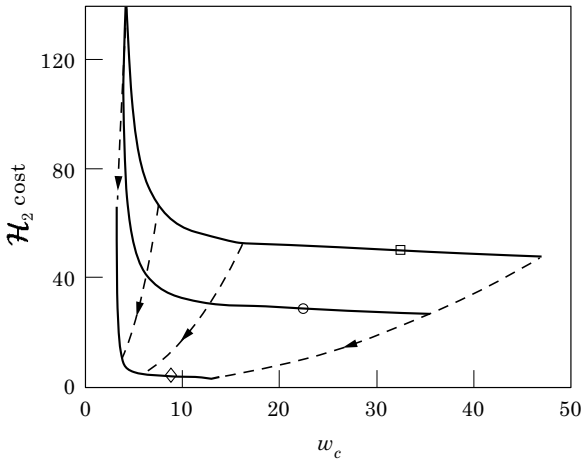

Figure 4. Comparison of the impact of reducing the noise of the feedback and feedforward sensors on the $\mathcal{H}_2$ performance and loop bandwidth. Solid lines show the trend as V_p decreases for various levels of V_{ms}: □, $V_{ms} = 10$; ○, $V_{ms} = 1$; ◇, $V_{ms} = 0{\cdot}1$. Dashed lines show the effect of hybrid configuration with arrows indicating the trend as feedforward sensor noise decreases.

performance decreasing from 140 to 50 as the intensity of the feedback sensor noise (V_p) decreases from 0·1 to 0·001, when the feedforward noise intensity is fixed at $V_{ms} = 10$. As expected, this improvement in feedback sensor quality results in a bandwidth increase from 4 to 47 rad/s. Note that, as illustrated in the figure, the ultimate levels of performance that can be achieved with this configuration are limited.

The figure also shows a key benefit of the hybrid $\mathcal{H}_2$ design in that it allows for simultaneous performance improvement and bandwidth reduction. The dashed lines in the figure show the effect of decreasing the feedforward signal noise V_{ms} for a fixed level of feedback sensor noise V_p. These dashed curves show that the $\mathcal{H}_2$ performance can be improved while simultaneously reducing the feedback control bandwidth, which is one of the key benefits of optimally blending the feedforward and feedback controllers. A typical trace indicates that a bandwidth reduction from 15 to 6 rad/s, a decrease of nearly 66%, is associated with a performance improvement from 55 to 5 as the feedforward noise, V_{ms} decreases from 10 to 0·1 and the feedback sensor noise intensity is kept constant at $V_p = 0{\cdot}03$.

This simple example illustrates the degree of coupling that occurs in the two control design problems. In particular, it shows how the feedback design is modified in the presence of a noisy feedforward sensor, and how optimal design blends in the feedforward component of the control to achieve improved performance. The key benefit of the combined design is that the bandwidth of the feedback component is reduced, thereby potentially providing improved stability robustness to high frequency unmodelled dynamics in the system. This additional design freedom is explored with a typical vibration isolation example in the next section.

4. EXAMPLE: ISOLATION SYSTEM WITH SENSOR DYNAMICS

This analysis can also be applied to the typical engineering problem of actively isolating a payload from the vibrations of a moving platform (see reference [16], for example). In this case active controller design fits into the hybrid control architecture when both the platform and the isolation mass are equipped with displacement sensors that have significant dynamics. This isolation system is considered in this section to further illustrate the advantages of the hybrid approach. In particular, the design approach offers the benefit of improved isolation performance using reduced feedback loop gain as compared to an equivalent LQG control augmented with a feedforward scheme that uses a rudimentary inversion of the feedforward sensor dynamics. The results that follow are presented in the same trade study manner as the preceding analysis, that is both $\mathcal{H}_2$ performance and bandwidth will be shown as functions of relative feedforward signal quality. This format clearly shows the synergistic trade-off that occurs between the feedforward and feedback controllers for the optimal isolation design.

The simple two sensor system is shown in Figure 5. The objective is to isolate the top mass M from the force disturbance due to ground motion w using the

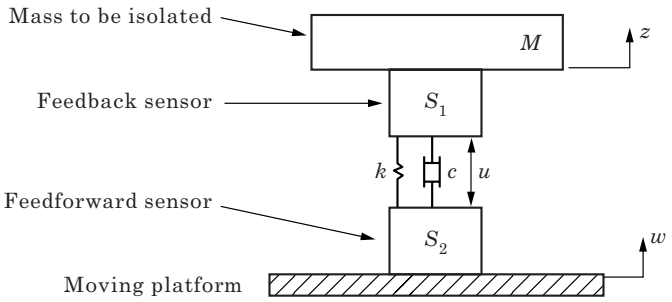

Figure 5. Isolation system schematic.

control force u. The ground motion couples to the mass through the mount which is modelled with a spring stiffness k and damping c. For this example the suspension parameters were chosen as $M = 1{\cdot}0$ kg, $k = 30$ N/m and $c = 0{\cdot}1$ N/m/s, which results in a lightly damped mode at $\omega_n = 5{\cdot}48$ rad/s.

Measurements of the top mass and the ground disturbance are provided by the two sensors, S_1 and S_2, respectively. The sensors considered are displacement seismometers that provide a measure of the displacement above the frequencies of the sensor internal resonance, which was chosen to be 1·0 rad/s (Figure 6). The sensors were therefore each modelled as a simple second order system, with both having a natural frequency at 1·0 rad/s, with S_1 and S_2 having 5 and 10% damping ratios, respectively. The hybrid controllers designed using the formulation given in section 2 are sixth order. In this study, the intensity of the feedback sensor S_1 was fixed at $V_p = 0{\cdot}05$, and the performance of the closed-loop system was evaluated for varying levels of feedforward sensor noise, V_{ms}.

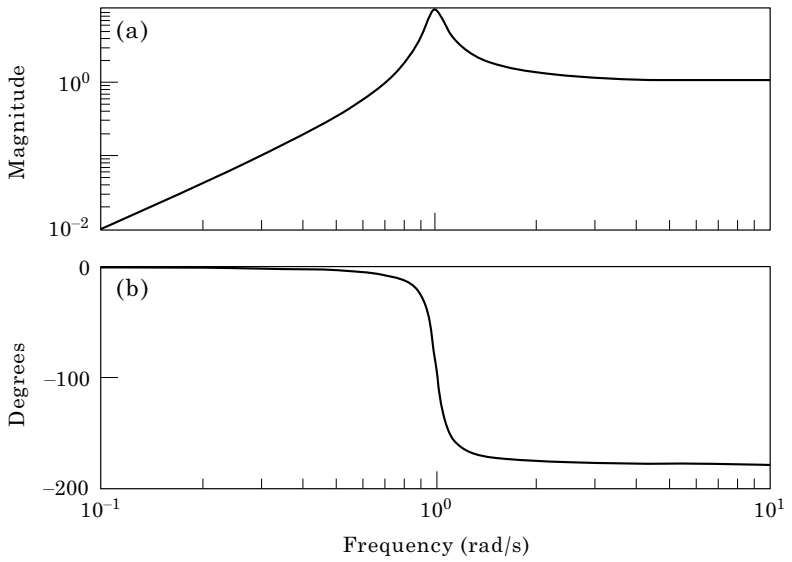

Figure 6. Frequency response of the displacement sensor dynamics: (a) amplitude response, and (b) phase response, as a function of frequency.

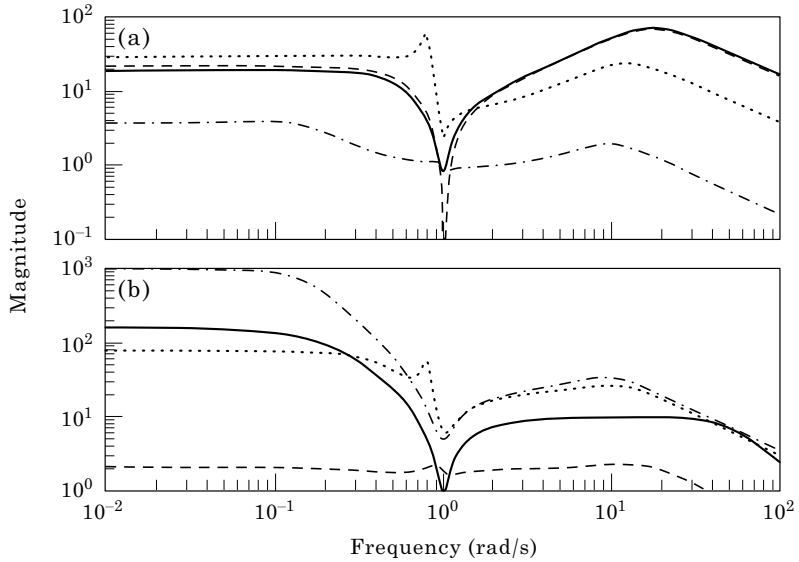

Figure 7. Feedback and feedforward transfer functions for various levels of V_{ms}: (a) feedback magnitude; $|K_{fb}(j\omega)|$; and (b) feedforward magnitude; $|K_{ff}(j\omega)|$. Solid lines: in (a) LQG feedback, in (b) manual feedforward design. Hybrid designs: –·–, $V_{ms} = 0{\cdot}005$; · · ·, $V_{ms} = 0{\cdot}066$; - - -, $V_{ms} = 8{\cdot}73$.

As a means of evaluation, the hybrid $\mathcal{H}_2$ controllers will be compared to a controller designed using a standard LQG feedback controller augmented with a *manual* feedforward compensator. This feedforward controller was designed by providing a stable, band-limited inversion of the feedforward sensor dynamics and injecting the signal into the closed-loop as a force command to complement the feedback control. This corresponds to a very effective engineering approach to the feedforward control that is commonly used in practice [17]. The magnitude of this feedback controller is plotted in Figure 7(a), and the manual feedforward transfer function is given in Figure 7(b). Also shown in the figure are the feedforward and feedback hybrid control magnitudes designed for various levels of V_{ms}. The trends uncovered in the previous section are clearly evident here. In particular, as the feedforward sensor noise is reduced, the feedback control magnitude decreases, particularly at high frequency, where the peak gain is nearly 80 when $v_{ms} = 8{\cdot}73$, down to 1·8 when the noise reduces to $v_{ms} = 0{\cdot}005$. Again, one also sees that as the feedforward noise levels increase the feedforward is, in essence, shut off, and the control reverts to the single sensor LQG design. This effect is seen in the figure by noting that the hybrid feedback control magnitude nearly traces over the single sensor feedback signal in Figure 7(a), while in Figure 7(b) the corresponding feedforward magnitude is reduced to a level near 2·0, when $v_{ms} = 8{\cdot}73$. The control plots, in a sense, justify the use of the manual feedforward. When the feedforward measurement is relatively noise-free, the hybrid feedforward control tends to invert the sensor dynamics in the same way in an effort to recover the sensor gain loss at low frequency, and to notch out the sensor peak at 1·0 rad/s.

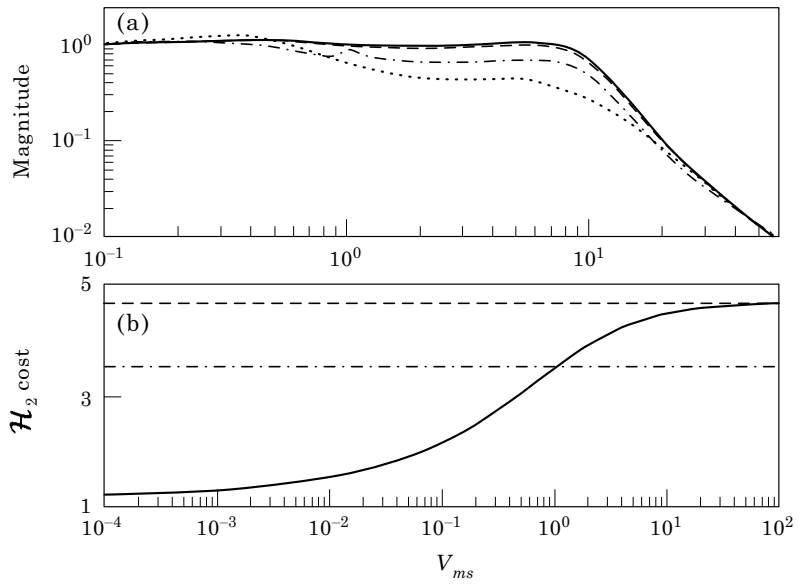

Figure 8. (a) Performance magnitude, $|G_{zw}|$ as function of frequency; —, LQG feedback only; –·–, LQC with manual feedforward; ···, hybrid ($V_{ms} = 0{\cdot}066$); - - -, hybrid ($V_{ms} = 8{\cdot}73$). (b) $\mathcal{H}_2$ cost versus sensor noise V_{ms}; —, hybrid designs; - - -, LQG only level; –·–, LQG with manual feedforward.

Figures 7(a) and 7(b) explicitly show the coupling discussed in section 2 that results in lower feedback gains, reduced bandwidth controllers, and increased use of the feedforward control as v_{ms} is reduced.

In Figure 8(a), the magnitudes of the closed loop response to disturbances, G_{zw}, are plotted. As expected, the hybrid controllers outperform the single sensor design when the feedforward signal has low noise, but this advantage diminishes as the quality of the feedforward measurement decreases. This is seen in two ways. First, the magnitude plots for the hybrid design and the single sensor design tend to merge as v_{ms} increases. For a value of $v_{ms} = 8{\cdot}73$ the graph of G_{zw} overlays the single sensor performance plot. Second, the $\mathcal{H}_2$ cost of the hybrid design asymptotes to the single sensor LQG level of 4·7 for high values of v_{ms}, as illustrated in Figure 8(b). It is interesting to note that the performance of the LQG design with the feedforward loop inserted actually outperforms the hybrid design when the noise levels of the feedforward sensor are above $v_{ms} = 1{\cdot}0$.

A secondary benefit to be gained with a hybrid design is in the possible reduction in loop gain. As before, one uses the crossover frequency of the loop transfer function, $K_{fb}G_{yu}$ to quantify this benefit. The bandwidth ω_b is defined as

$$\omega_b = \min\{\omega_0 \mid |K_{fb}G_{yu}(\mathrm{j}\omega)| < 0{\cdot}707, \quad \forall\omega \geqslant \omega_0\}.$$

This performance measure clearly has important implications for the stability robustness of the system that can be expected in the presence of unmodelled high frequency dynamics. In particular, reducing ω_b could mean that the system is much less susceptible to a destabilizing interaction with the uncertain modes of the system at high frequency. In Figure 9(a), the magnitudes of the loop transfer

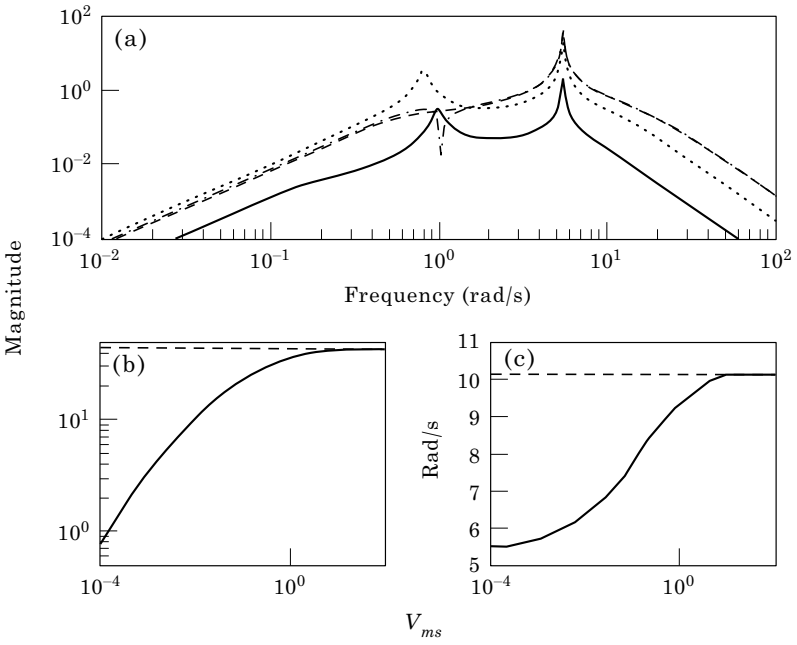

Figure 9. (a) Loop transfer function, $|K_{fb}G_{yu}|$, as function of frequency; —, hybrid $V_{ms} = 0{\cdot}005$; ···, hybrid $V_{ms} = 0{\cdot}066$; –·–, hybrid $V_{ms} = 8{\cdot}73$; - - -, LQG only design. (b) Peak loop gain versus sensor noise V_{ms}; —, hybrid designs; - - -, LQG only level. (c) Bandwidth ω_b with V_{ms}; —, hybrid designs; - - -, LQG only level.

functions are graphed for various levels of V_{ms}. As shown, the overall gain decreases as the feedforward sensor noise decreases. The peak gains reduce from a value of 43 for $V_{ms} > 10$ to less than unity for $V_{ms} < 0{\cdot}004$, as indicated in Figure 9(b). Again, consistent with the analysis given for the scalar system, the highest levels of loop gain and ω_b are given for the single sensor LQG design, and effective reduction of these numbers can be achieved using the hybrid design with improving feedforward signal quality. For the example considered, ω_b is reduced from LQG loop bandwidth of 10·1 rad/s to 6·2 by using a feedforward sensor with $V_{ms} = 0{\cdot}01$, as shown in Figure 9(c).

The isolation design for this system clearly demonstrates the key benefit of the hybrid architecture of simultaneous $\mathcal{H}_2$ performance improvement and reduced control bandwidth. Here, the inclusion of the feedforward sensor into the design allows a bandwidth reduction from 10·1 to 6·2 rad/s while giving a factor of 3 improvement in $\mathcal{H}_2$ performance.

5. CONCLUSIONS

This paper extends previous analyses of $\mathcal{H}_2$ optimal hybrid controllers that use both feedforward and feedback sensors. Prior results have demonstrated that the two control design problems (feedforward and feedback) are separable for the special case of a noise-free feedforward sensor. This paper shows that stronger

coupling exists between the feedback and feedforward controllers when there is noise on the feedforward sensor. This coupling is a result of the effective change in the process noise associated with the measured disturbance that is achieved when the feedforward sensor noise is modified. The analysis in the paper shows that reducing the feedforward sensor noise results in a lower feedback loop gain, a slower controller pole, and an increased use of the feedforward controller. Several examples are presented to show that the hybrid architecture can be used to simultaneously design for both improved optimal $\mathcal{H}_2$ performance and reduced closed-loop bandwidth. These examples provide further insight on the synergistic coupling that exists between the feedback and feedforward control designs, and the potential advantages of this coupling in terms of improved robustness to uncertain high frequency dynamics.

6. SUMMARY

The design of controllers using both feedback and feedforward sensors has been called *hybrid* control. Within this framework, the feedback sensor is used primarily for stabilization while the feedforward sensor is used to improve the disturbance rejection performance of the system. This paper analyzes the simultaneous design of the feedforward and feedback controllers within this architecture. Prior results have demonstrated that these two control design problems (feedforward and feedback) are separable for the special case of a noise-free feedforward sensor. This separation means that the feedback controller can be designed independently of the feedforward controller. This paper extends the analysis to consider the more realistic case with a noisy feedforward sensor. Including this sensor noise enables a more complete investigation of the strong coupling that typically exists between the feedforward and feedback components of the architecture. The results show how the combined controller can be synergistically used to simultaneously design for both optimal vibration performance and reduced closed-loop bandwidth.

ACKNOWLEDGMENT

The authors greatly appreciate the preprint copy of the conference paper [4] provided by Professor Dennis Bernstein.

REFERENCES

1. R. L. CLARK 1995 *Journal of Dynamic Systems, Measurement and Control* **117**, 232–240. A hybrid autonomous control approach.
2. W. R. SAUNDERS, H. H. ROBERTSHAW and R. BURDISSO 1996 *Noise Control Engineering Journal* **44**, 11–21. A hybrid structural control approach for narrow-band and impulsive disturbance rejection.
3. S. J. ELLIOT and T. J. SUTTON 1996 *IEEE Transactions on Speech and Audio Processing* **4**, 214–223. Performance of feedforward and feedback systems for active control.

4. D. S. BERNSTEIN and R. L. CLARK 1998 *Proceedings of the American Control Conference*. Hybrid control for vibration and acoustics. (Accepted for publication in *Journal of Sound and Vibration*.)
5. C. R. FULLER, S. J. ELLIOT and P. A. NELSON 1996 *Active Control of Vibration*. London: Academic Press.
6. J. C. DOYLE and G. STEIN 1981 *IEEE Transactions on Automatic Control* **26**, 4–16. Multivariable feedback design: concepts for a classical/modern synthesis.
7. S. SKOGESTAD and I. POSTLETHWAITE 1996 *Multivariable Feedback Control: Analysis and Design*. New York: Wiley.
8. G. J. BALAS, J. C. DOYLE, K. GLOVER and A. PACKARD 1993 *μ—Analysis and Synthesis ToolBox*. Natick, MA: The Mathworks.
9. D. BANJERDPONGCHAI and J. P. HOW 1996 *AIAA Guidance, Navigation, and Control Conference*, AIAA-96-3733. Parametric robust $\mathcal{H}_2$ control design using LM1 synthesis.
10. K. Y. YANG, G. LIVADAS and S. R. HALL 1996 *AIAA Guidance, Navigation, and Control Conference*, AIAA-96-3731. Using linear matrix inequalities to design controllers for robust $\mathcal{H}_2$ performance.
11. L. A. SIEVERS, G. H. BLACKWOOD, G. H. MERCADAL and A. H. VON FLOTOW 1991 *Proceedings of the American Control Conference* **2**, 1353–1359. MIMO narrow-band disturbance rejection using frequency shaping of cost functionals.
12. D. G. MACMARTIN, S. R. HALL and D. MUSTAFA 1991 *Proceedings of the American Control Conference* **2**, 1353–1359. On a cost function for $\mathcal{H}_2/\mathcal{H}_\infty$ minimization
13. N. K. GUPTA 1980 *Journal of Guidance and Control* **3**, 529–535. Frequency–shaped cost functionals: extension of linear quadratic Gaussian methods.
14. P. COLANERI, J. C. GEROMEL and A. LOCATELLI 1997 *Control Theory and Design: an RH_2 and RH_∞ Viewpoint*. London: Academic Press.
15. S. P. BOYD and C. H. BARRATT 1991 *Linear Controller Design: Limits of Performance*. Englewood Cliffs, New Jersey: Prentice-Hall.
16. M. E. REGELBRUGGE, A. CARRIER and W. C. DICKSON 1996 *Journal of Intelligent Material Systems and Structures* **7**, 211–217. Performance of a smart vibration isolator for precision spacecraft instruments.
17. D. DE BRA 1997 Personal communication, Stanford University.